30th NATIONAL RADIO SCIENCE CONFERENCE
(NRSC 2013)
April 16-18, 2013, National Telecommunication Institute, Egypt

K2. Motion Estimation for Ultrasound Elastography Using Optimized Block Matching with Lateral Continuity Correction

Marwan H. Hussein, Yasser M. Kadah
Biomedical Engineering Department, Cairo University, Giza, Egypt, Email: eng.marwan.h.hussein@gmail.com

ABSTRACT

The displacement estimation phase in ultrasound elastography is similar to the motion estimation problem in the video compression domain. Block matching can then be applied to successive ultrasound radio frequency frames to get displacement fields. We utilize the inherent continuity in the soft tissue to apply an optimized version of exhaustive block matching to elasticity phantoms to generate displacement fields. Furthermore, we impose lateral continuity on displacements of each row in the reference image to remove false peaks in the optimized exhaustive search. Application of Linear least squares differentiation to the resultant axial displacement field yields promising results. The resultant strain field is comparable to a published result. We present quantitative assessment for the resulting displacement fields and the runtime of the motion estimation algorithms.

Keywords: *Ultrasound (US) elastography, motion estimation, displacement field, block matching algorithms (BMAs), exhaustive search (ES), lateral continuity correction (LCC).*

I. INTRODUCTION

Ultrasound (US) elastography has been a potential medical imaging topic for research and application for about 20 years[1], [2]. Many variations of US elastography exist and they are mainly categorized into static and dynamic techniques[1], [2], [3]. We focus on static US elastography introduced by Ophir[4]. In this technique an external quasi-static compression is applied axially to the tissue to acquire successive RF frames. Then, pre and postcompression frames are compared to generate a displacement field which is further processed to get a strain profile (for example by applying spatial derivation). This strain profile can be used qualitatively to differentiate hard and soft areas even if they are isoechoec. This is possible because hard areas (which can represent lesions or tumors) experience less strain than soft areas. Furthermore, the inverse Hooke's law problem can be solved to get quantitative elasticity measures (elasticity moduli)[5].

Many approaches to displacement estimation in US elastography exist. Some of these approaches are based on windowed cross correlation [4]. Others tackle the displacement estimation as an optimization problem[6]. It can be noticed that this estimation problem is similar to the motion estimation phase in video compression domain (e.g. MPEG compression). Although some differences exist between the natures of the ultrasonic image and the photographic image[7], block matching algorithms (BMAs), used with photographic images, can be used with US radio frequency frames to generate displacement fields.

In this work, we propose a modified version of one of the BMAs. This modification makes the BMA more oriented to work with US data. We also utilize the inherent continuity in the imaged tissue to make an optimized version of the previously modified BMA. This continuity criterion accounts for the axial continuity, so we add a lateral continuity correction step to remove false peaks along the horizontal direction and enhance the resultant fields.

II. METHODS

The general block diagram of our system is shown in Fig. 1. For testing purpose we used the same phantom RF data in Rivaz et al. as the input to our algorithm[6], [8]. The B-mode images for pre and postcompression frames (by demodulating RF frames) are shown in Fig. 2. The RF frames were then cropped to have appropriate data size for testing (as shown in Fig. 2). Then, both images were input to the motion estimation algorithm.

A. Modified Exhaustive Search (ES)

We used one of the BMAs (commonly used in video compression domain) to estimate the displacement field of the precompression image. In the video compression domain, where the video is a series of frames, BMAs are

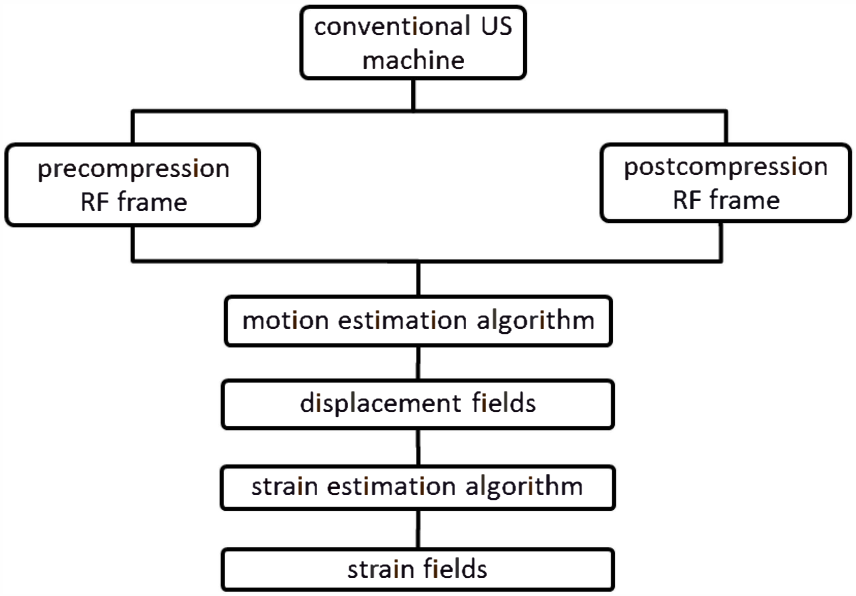

Fig. 1. General block Diagram of US elastography based on block matching of RF images

based on dividing a frame into a matrix of non-overlapping square macro blocks and each block is compared with the corresponding block and its adjacent neighbors in the previous frame to create a vector that represents the movement of a macro block in the previous frame from one location to another in the current frame. This movement, calculated for all the macro blocks comprising a frame, constitutes the displacement field.

The search criterion between blocks is based on minimizing a cost function. The searched block that generates the least cost is considered the best match for the reference block. Two cost functions are frequently used due to their simplicity, namely Mean Absolute Difference (MAD) and Mean Squared Error (MSE) given by the following equations:

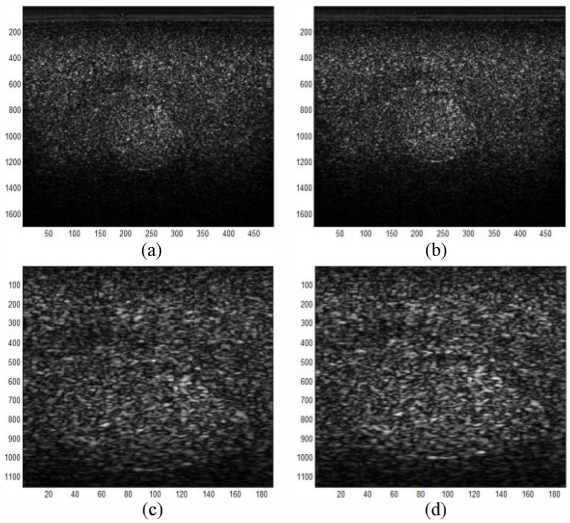

Fig. 2.Phantom B-mode images. (a) Precompression. (b) Postcompression. (c) Precompression (after cropping). (d) Postcompression (after cropping). The size of both cropped images is 1151*188 pixels. The semicircular lesion can be failry seen (isoechoec with surrounding tissue).

$$MAD = \frac{1}{N^2}\sum_{i=0}^{N-1}\sum_{j=0}^{N-1}\left|G_{ij} - \grave{G}_{ij}\right| \quad (1)$$

$$MSE = \frac{1}{N^2}\sum_{i=0}^{N-1}\sum_{j=0}^{N-1}\left(G_{ij} - \grave{G}_{ij}\right)^2 \quad (2)$$

where$N$ is the side of the macro bock, G_{ij} and $\grave{G}_{ij}$ are the pixels being compared in the reference macro block and searched macro block, respectively. The formula for the BMA is

$$MAD(m,n) = \frac{1}{N_1 N_2}\sum_{j=-\frac{N_2-1}{2}}^{\frac{N_2-1}{2}}\sum_{i=-\frac{N_1-1}{2}}^{\frac{N_1-1}{2}}\left|G(I+i,J+j) - \acute{G}(I+i+m,J+j+n)\right| \quad (3)$$

where(m,n) is the search location(limited by the search range$p$), $N_1$and$N_2$are the horizontal and vertical block dimensions respectively, (I,J) is the location of the center of the reference image block.

For our application (US elastography),the search parameter p was initially set to 5 (the idea is represented in Fig. 3(a)). There are various techniques for block matching which differ in accuracy and speed[9], but we chose to start with the most computationally expensive, yet most accurate, algorithm - the exhaustive search (ES), to assess the quality of motion fields generated using BMAs with RF data.

After compressing the imaged tissue by the probe, the distance between any locus in the tissue and the probe gets smaller. Consequently, every locus appears in an upper location in the postcompression image than its original location in the precompression image. Utilizing this, and because we were using the postcompression image as the reference image, we applied a modification to the ES algorithm in which we limit the search range vertically to the lower half of the search window (see Fig. 3(b)). We expected this modification to enhance the quality of the displacement field (besides enhancing speed definitely) as it should reduce false positives.We set the vertical search range for ES to the applied axial compression depth (as it is the upper limit) according to the following formula:

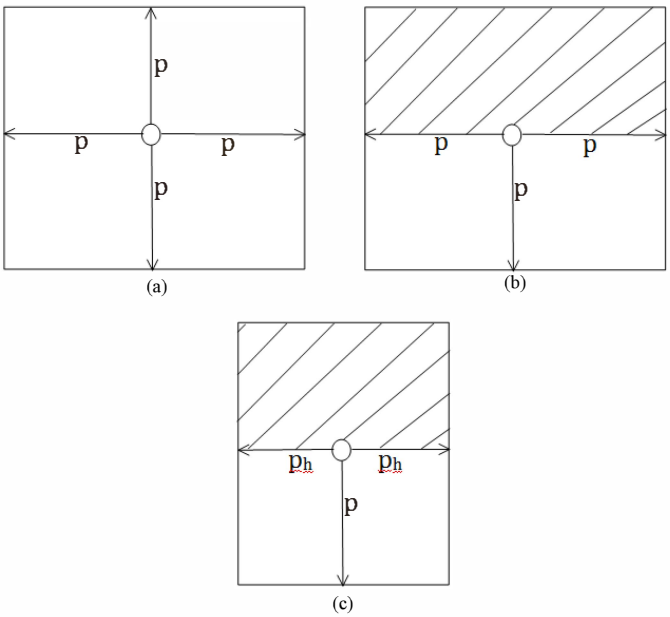

Fig. 3.ES with modifications. (a) Basic ES. (b) ES with the first modification (lower-only search). (c) ES with the two modifications (lower-only and less horizontal search). In all configurations p represents the vertical search range and p_h represents the horizontal search range (which typically should be less than$p$).

$$applied\ compression\ [samples] = applied\ compression\ [m] \times \frac{2 \times sampling\ freq\ [sample/sec]}{propagation\ speed\ (1540)\ [m/sec]} \quad (4)$$

The values of sampling freq (40 Mhz) and physical applied axial compression (0.2 inch). According to Eq. 3, the applied compression in samples was 264 and thus, even if this search range theoretically should contain any motion vectors, getting a result using such a huge search range is hard for a serial implementation of the ES algorithm.

An additional property of elastography images is that the majority of the displacement should be in the vertical (axial) direction due to the nature of the compression (which is axial). This let us apply an additional modification to the ES algorithm in which we limited the search range in the horizontal (lateral) direction (as shown in Fig. 3(c)) where p_h is the horizontal search parameter. Typically p_h should be less than p(we set $p_h$to 2). Again we expected this to further reduce false positives in addition to enhancing speed.

B. Optimized ES (Exploiting Tissue Continuity)

A main problem facing application of conventional ES to elastography data (even after previous two modifications) is that the continuity of displacement fields (as the tissue is a continuum) is not exploited by conventional ES. This results in noisy displacement fields with no continuity and with false peaks (especially when the search range is big) in addition to long search time.

To solve this problem, it is stated in [6]that due to the continuity of motion and low value of applied strain, movement of adjacent regions in the RF frame should not vary significantly. We applied the same concept to the BM problem as follows: let that the axial displacement of location (I,J)in the RF frame be$d_{axl}(I,J)$, then we can confine the search range for the axial displacement of the lower sample, $(I,J+1)$, to $d_{axl}(I,J)-1$, $d_{axl}(I,J)$, $d_{axl}(I,J)+1$. This is equivalent to limiting the search range for the lower sampleto 1 sample in the 4 directions provided that the search center is now updated with the displacement of the upper sample (i.e. the new search center is $\big(I,J+1+d_{axl}(I,J)\big)$, not $(I,J+1)$). Applying the same concept to lateral displacement, then we could confine the search range for displacement of location $(I,J+1)$, to a 3-by-3 window centered at the location guided by the already-estimated displacement of the adjacent (upper) sample. This guided location is$\big(I+d_{lat}(I,J),J+1+d_{axl}(I,J)\big)$.This idea can be expressed mathematically by changing the original formula of block matching fromEq. 3 to

$$MAD(m,n) = \frac{1}{N_1 N_2} \sum_{j=-\frac{N_2-1}{2}}^{\frac{N_2-1}{2}} \sum_{i=-\frac{N_1-1}{2}}^{\frac{N_1-1}{2}} \left| G(I+i,J+1+j) - \acute{G}(I+d_{lat}(I,J)+i+m,J+1+d_{axl}(I,J)+j+n) \right| \quad (5)$$

To apply the previous idea, one should estimate the displacement field for the first row in the reference image then use this estimate as a basis for the lower rows. So, we didmodified ES for the first row (as no priori are found yet) then usedthe resultant displacement vectors to guide the search for displacements of lower samples.

We implemented this modification using the axial search range calculated by Eq. 3 for the first row for full search and using a lateral search range = 10 A-lines (empirical).

C. Lateral Continuity Correction (LCC)

Results of the previous correction showed that resultant displacement fields exhibit axial smoothness but not lateral smoothness. Examining the displacement estimates for the first row (estimated with full search) show that some false peaks appear. This is due to the large search region in the axial direction. Consequently, these errors shall propagate to the estimates of the lower rows due to the dependency in this guided technique. We tried to solve this problem by applying 1D median filtration to the displacement estimates of the first row to remove the outliers (false detections) before proceeding to the lower rows. The result for 1-by-15 median filtration applied to

the displacements of first row is shown in the results section. Also, we applied the same filtration but to the displacements of all rows in the reference image.

III. RESULTS

For qualitative assessment, the resulting vertical displacement fields (absolute values) for the modified ES, optimized ES, optimized ES with LCC (applied to first row and all rows) are shown in Fig.4(a-d) respectively. The block size used is 9-by-5[1](empirical). The strain field generated from the displacement field of the optimized ES with LCC (applied to all rows) using linear LSQ differentiator(as in [6]) is shown in Fig. 5(a).The strain field generated by [8] is also shown in Fig. 5(b) for comparison with our strain field.

We chose a unitless measure for quantitative assessment of motion fields. That is the signal-to-noise ratio (SNR) defined by the following equation:

$$SNR = \frac{\bar{s}}{\sigma} \tag{6}$$

where$\bar{s}$ and σ are the spatial average and standard deviation of the displacement field.The runtime[2] of the motion estimation block (t_{ME}), the SNR for the vertical displacement field (SNR_V) are shown in Table I for the fourES configurations.

IV. DISCUSSION

Fig. 4(a) shows that modified ES does not produce a meaningful motion field. This can be understood because the search ranges are empirical and small, so the search window may not contain the corresponding block for the current reference block. Also, The modified ES does not exploit the inherent tissue continuity and thus may be subject to false detections. Fig. 4(b) shows that axial displacement field undergoes axial continuity after imposing continuity condition in this algorithm (optimized ES). Although search window for the first row of the reference image is larger than that for the modified ES, Table 1 shows that the time for the optimized ES is overall less than that of modified ES. This is because full search is done only for the first row, then the search region is reduced to 3-by-3 only for the rest of the reference samples. However, It can be seen that the axial displacement undergoes lateral discontinuity. The reason for this is that the large search region for the first row leads to some false peaks appearing in the displacement estimation of the first row. Since this estimation is used to guide the search for the lower row (and so on), the false peaks propagate along the axial direction.

Although the results for the optimized ES with LCC (all rows) look promising and the SNR_v for this configuration is the highest among the four ES configurations (as shown in Table 1),some errorsexist in the

TABLE I. QUANTITATIVE MEASURES FOR THE DIFFERENT ES CONFIGURATIONS

Measure	Modified ES	Optimized ES	Optimized ES with LCC (1st row)	Optimized ES with LCC (all rows)
t_{ME} (s)	55.39	29.92	30.19	30.55
SNR_v	1.49	0.77	0.72	1.98

[1] For US, the block height should be bigger than block width because the ultrasonic RF signal has a higher resolution in the axial direction than the lateral direction, and the strain generated is expected to be mainly along the axial direction.
[2] All algorithms are implemented in MATLAB 2012a and tested on a 2.2 GHz CPU.

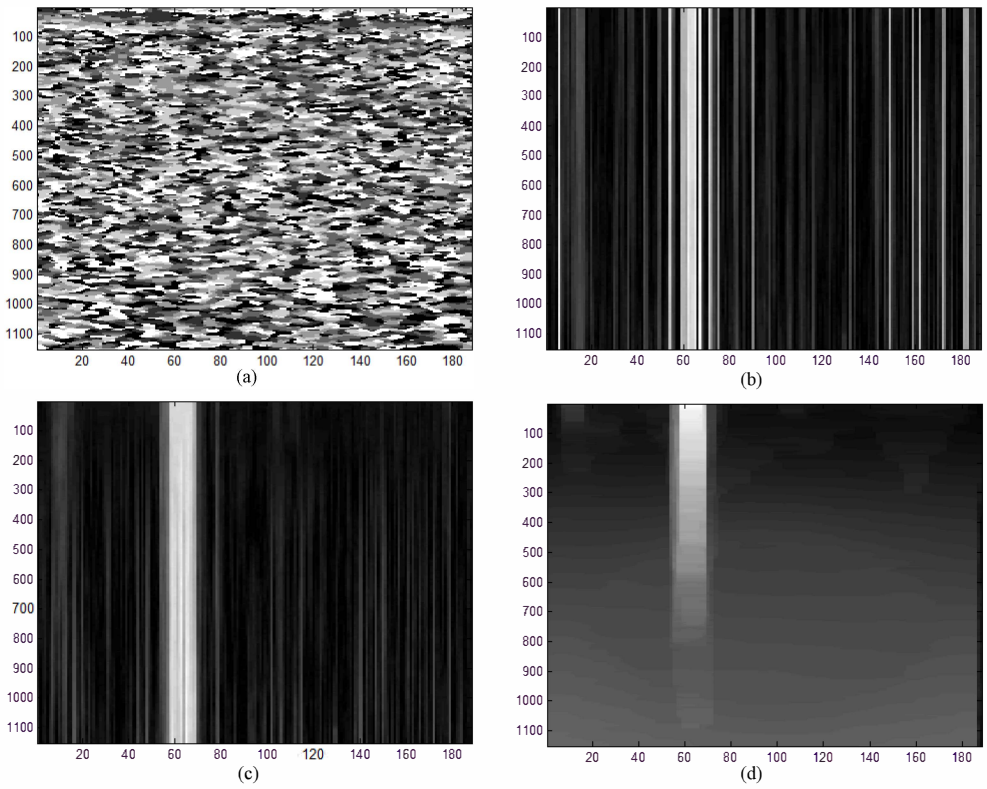

Fig. 4. Axial displacement fields for the four ES configurations. (a) modified ES. (b) Optimized ES. (c) Optimized ES with LCC (1st row). (d) Optimized ES with LCC (all rows).

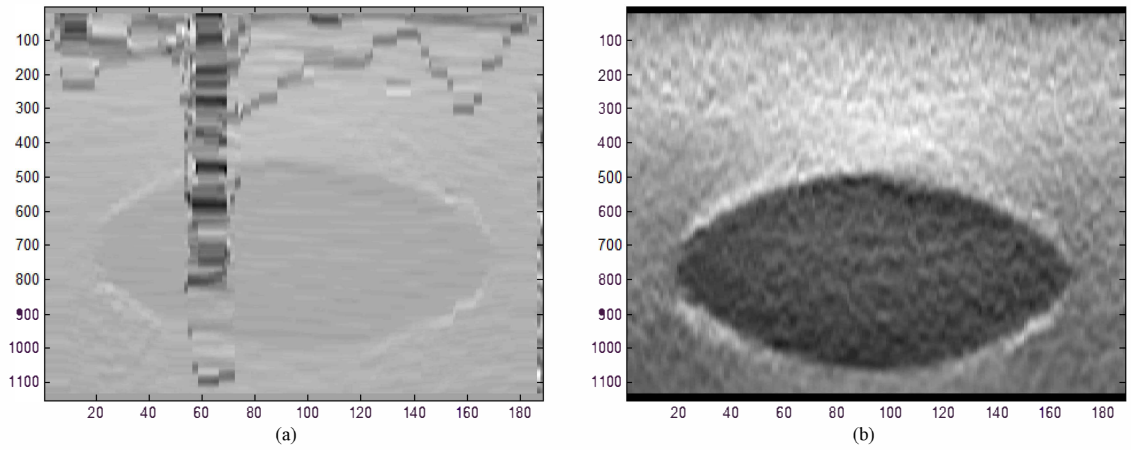

Fig. 5. Axial strain fields using linear LSQ differentiation. (a) Using displacement field from our algorithm (Optimized ES with LCC (all rows)). (c) Using displacement field from [2].

displacementand strain fields (Fig. 4(d) and 5(a)). It should be considered that the median filtration used is a naïve empirical salt and pepper noise removal technique, and thus may not be the best choice for false peaks removal. Other techniques may be better for this purpose. Concerning performance, the runtime for the optimized ES with LCC (all rows) is nearly the same as that of the optimized ES (without LCC) despite application of median filtration to each row of the reference image (This is shown in Table 1). However, this performance (30 secs) is not yet suitable for real time applications and further performance enhancement is required.

Many points are potential to future work. To enhance the quality of displacement and strain fields, we can experiment with a better technique to remove outliers from the displacement estimates of each row. This can be done, for example, by robust fitting of displacements to get a base curve then removing outliers based on difference with this baseline curve. Once the outliers are removed, we can interpolate the values of the removed false detections. Also, we can make the block size for ES a function of imaging parameters and we can similarly make the lateral search region for the first row (full search) in the optimized ES with LCC a function of imaging parameters and applied compression. This will be better than setting these values empirically. Clinical trials with more quantitative measures are needed to better assess the performance of our algorithm.

To enhance the runtime of the algorithm, several approaches are possible. We can use non-overlapping blocks for the reference image (like the case in MPEG motion estimation) to enhance speed then interpolate the displacement of skipped positions. Another approach is to apply motion estimation algorithm to undersampled versions of the RF frames then upsample the resulting displacement fields. A third approach is to make a parallel implementation of the motion estimation algorithm to leverage the power of multiple CPUs and GPUs (a similar approach is done in [10])

V. Conclusion

We presented an optimized version of the ES algorithm that exploits the inherent continuity in the successive US images to generate displacement fields. The proposed algorithm was applied to elasticity phantom data. Results indicate that this direction is promising. Further future work was discussed that can enhance both the quality and the runtime of the optimized ES algorithm.

References

[1] P. R. Hoskins, K. Martin, and A. Thrush, *Diagnostic ultrasound: physics and equipment*: Cambridge University Press, 2010.

[2] K. Parker, M. Doyley, and D. Rubens, "Imaging the elastic properties of tissue: the 20 year perspective," *Physics in Medicine and Biology,* vol. 56, p. R1, 2010.

[3] J. Ophir, S. Alam, B. Garra, F. Kallel, E. Konofagou, T. Krouskop, and T. Varghese, "Elastography: ultrasonic estimation and imaging of the elastic properties of tissues," *Proceedings of the Institution of Mechanical Engineers, Part H: Journal of Engineering in Medicine,* vol. 213, pp. 203-233, 1999.

[4] J. Ophir, I. Cespedes, H. Ponnekanti, Y. Yazdi, and X. Li, "Elastography: a quantitative method for imaging the elasticity of biological tissues," *Ultrasonic imaging,* vol. 13, pp. 111-134, 1991.

[5] A. Skovoroda, S. Emelianov, and M. O'Donnell, "Tissue elasticity reconstruction based on ultrasonic displacement and strain images," *Ultrasonics, Ferroelectrics and Frequency Control, IEEE Transactions on,* vol. 42, pp. 747-765, 1995.

[6] H. Rivaz, E. Boctor, P. Foroughi, R. Zellars, G. Fichtinger, and G. Hager, "Ultrasound elastography: a dynamic programming approach," *Medical Imaging, IEEE Transactions on,* vol. 27, pp. 1373-1377, 2008.

[7] F. Yeung, S. F. Levinson, D. Fu, and K. J. Parker, "Feature-adaptive motion tracking of ultrasound image sequences using a deformable mesh," *Medical Imaging, IEEE Transactions on,* vol. 17, pp. 945-956, 1998.

[8] H. Rivaz, E. M. Boctor, M. A. Choti, and G. D. Hager, "Real-time regularized ultrasound elastography," *Medical Imaging, IEEE Transactions on,* vol. 30, pp. 928-945, 2011.

[9] A. Barjatya, "Block matching algorithms for motion estimation," ed: unpublished.

[10] X. Yang, S. Deka, and R. Righetti, "A hybrid CPU-GPGPU approach for real-time elastography," *Ultrasonics, Ferroelectrics and Frequency Control, IEEE Transactions on,* vol. 58, pp. 2631-2645, 2011.